ACS APPLIED MATERIALS & INTERFACES

Research Article

www.acsami.org

Proton Conducting Self-Assembled Metal–Organic Framework/Polyelectrolyte Hollow Hybrid Nanostructures

Unal Sen,[*,†,‡] Mustafa Erkartal,[§] Chung-Wei Kung,[‡,∥] Vijay Ramani,[⊥] Joseph T. Hupp,[*,‡] and Omar K. Farha[*,‡,#]

[†]Department of Mechanical Engineering and [§]Department of Materials Science and Nanotechnology Engineering, Abdullah Gül University, 38080 Kayseri, Turkey

[‡]Department of Chemistry, Northwestern University, 2145 Sheridan Road, Evanston, Illinois 60208, United States

[∥]Department of Chemical Engineering, National Taiwan University, Taipei 10617, Taiwan

[⊥]Center for Electrochemical Science and Engineering, Department of Chemical and Biological Engineering, Illinois Institute of Technology, 10 West 33rd Street, Chicago, Illinois 60616, United States

[#]Department of Chemistry, Faculty of Science, King Abdulaziz University, Jeddah, Saudi Arabia

Supporting Information

ABSTRACT: Herein, a room temperature chemical process to synthesize functional, hollow nanostructures from zeolitic imidazolate framework-8 (ZIF-8) and poly(vinylphosphonic acid) (PVPA) is reported. Syntheses are initiated by physically blending the components—a process that is accompanied first by encapsulation of ZIF-8 crystallites by PVPA and then by fragmentation of the crystallites. The fragmentation process is driven by partial displacement of the methyl-imidazolate ligands of Zn(II) in ZIF-8 by phosphonate groups on PVPA. Differences in rates of diffusion for the components of the reactive mixture yield a Kirkendall-like effect that is expressed as a hollow-particle morphology. The obtained hollow nanostructures feature hybrid shells containing PVPA, ZIF-8, and their cross-reacted products. The hybrid structures display substantial proton conductivities that increase with increasing temperature, even under the anhydrous conditions prevailing at temperatures above the boiling point of water. For example, at T = 413 K the proton conductivity of ZIF-8@PVPA reaches 3.2 (±0.12) × 10^{-3} S cm^{-1}, a value comparatively higher than that for PVPA (or ZIF-8) in isolation. The high value may reflect the availability in the hybrid structures of free (and partially free), amphoteric imidazole species, and their hydrogen-bonding interactions with phosphonate and/or phosphonic acid units. The persistence of ample conductivity at high temperature reflects the elimination of phosphonic acid group dehydration and dimerization—an effect that strikingly degrades the conductivity of pure PVPA under anhydrous conditions.

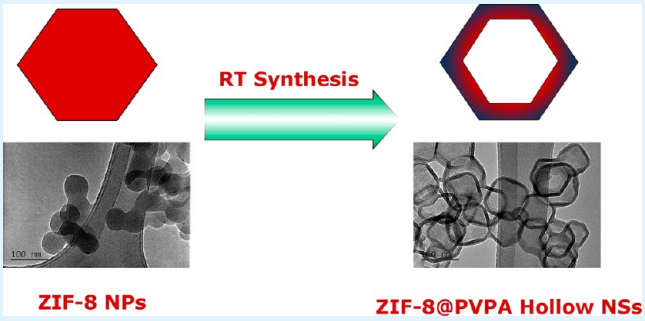

KEYWORDS: *ZIF-8, PVPA, hollow nanostructures, proton conductivity, fuel cell*

1. INTRODUCTION

Proton conducting materials have become the focus of intensive research efforts due to their potential applications in fuel cells, gas sensing, and contaminant removal.[1] A proton exchange membrane fuel cell (PEMFC) is a promising device that can supply electrical energy with high efficiency and very low environmental impact. In a typical PEMFC, a polymeric electrolyte membrane is the physical core of the device and selectively allows proton transport from anode to cathode. Commercial state-of-the-art electrolyte membranes are based on perfluorosulfonic acid polymers, e.g., Nafion, which can achieve a proton conductivity on the order of 10^{-1}–10^{-2} S cm^{-1} at 80 °C under high relative humidity (98% RH).[1,2] The conductivity drops significantly under conditions of lower hydration, however, and can be nearly zero under truly anhydrous conditions.[3] Therefore, much attention has been paid to the development of new membranes for PEMFCs that can operate at high temperatures and low relative humidity.[3] Proton carriers other than water, including nonvolatile acids (such as H_3PO_4 or R-PO_3H_2)[4,5] and organic heterocycles (such as imidazole and triazole),[6−9] have been introduced to enhance anhydrous proton conduction, since these materials can provide a dynamic hydrogen bonding pathway with pronounced amphoteric behavior, simultaneously acting as proton donor and proton acceptor.

Metal–organic frameworks (MOFs), also known as crystalline/amorphous coordination polymers or porous coordination networks, are crystalline porous compounds that are con-

Received: May 18, 2016
Accepted: August 19, 2016
Published: August 19, 2016

DOI: 10.1021/acsami.6b05901
ACS Appl. Mater. Interfaces 2016, 8, 23015−23021

structed using metal ions/clusters and organic ligands (linkers).[10−14] The strong coordination bonds between the metal and ligand constituents result in the formation of 2-D or 3-D extended infinite networks.[11] Owing to their highly porous structures and uniformity, MOFs have attracted substantial attention for potential applications in gas storage[15−18] and catalysis.[19−21] Up until now, the proton conductivity values of the MOFs reported in the literature have been highly humidity dependent since the proton conduction occurs in the presence of water molecules as proton carriers within a hydrogen-bonded network.[22−26] Several studies have reported that appropriately chosen MOFs can show considerable proton conductivity above 100 °C.[27−29] Doping MOFs with acids and embedding protogenic reagents into MOFs have been shown to considerably increase proton conductivity above 100 °C and under very low humidity conditions.[22,30,31] When blended with organic polymers, MOFs typically exhibit good interfacial compatibility, reflecting the high compatibility of the polymer with the organic ligands in the framework.[32] These observations suggest that exploration of composite materials based on MOF/polymer hybrids may yield good proton-conducting structures. Nevertheless, relatively little has been published on proton conduction by polymer/MOF hybrids. Liang et al. reported on proton conduction under low humidity by a 2D-MOF/PVP hybrid.[33] Xu et al. studied oriented, electrospun MOF/polymer nanocomposite membranes and showed that proton conductivity values for the studied structure are about 10^{-2} S cm^{-1} at 160 °C under anhydrous conditions.[34]

Poly(vinylphosphonic acid) (PVPA) shows considerable advantages for use in fuel cell electrolytes when compared to liquid heterocycles such as imidazole and pyrazole.[35] Previous researchers[4,5,36] have documented that the proton conductivity of pure PVPA is relatively high owing to the amphoteric behavior of phosphonic acid groups ($-PO_3H_2$) and their ability to hydrogen bond. Notably, the strong carbon−phosphorus bond enhances the thermal stability of the polymer for high temperature operation. PVPA is also an appropriate and useful alternative material to phosphoric acid, which is commonly used as a dopant acid in acid−base complexes, due to the high concentration of immobilized phosphonic acid groups. However, the proton conductivity of PVPA can depend strongly on temperature. Briefly, the conductivity of PVPA can be inhibited by self-condensation (i.e., phosphoanhydride formation). The equilibrium between condensed (anhydride) and noncondensed forms of the phosphonic acid units depends strongly on water content within the polymer. At temperatures above 100 °C, water content within a membrane typically drops drastically. For PVPA membranes, the drop is accompanied by self-condensation and a corresponding reduction in the number of phosphonic acid sites. In turn, the proton conductivity of the polymer decreases. To avoid the undesired formation of phosphonic anhydride species, molecular-scale spacers are typically introduced between the polymer's phosphonic acid units.[4,5,35,37]

Previously, we reported the enhancement in proton conductivity elicited by embedding the MOF, ZIF-8 (Zeolitic Imidazolate Framework 8), in a polymer matrix.[32] In the present work, hollow nanostructures composed of PVPA and ZIF-8 (designated ZIF-8@PVPA) have been successfully synthesized and tested as new proton conductors. To the best of our knowledge, this is one of the first reports describing the synthesis of a hollow nanostructured hybrid material consisting of a MOF and polymer.[38] The two constituents were mixed in either of two formula-unit ratios to obtain the hybrid materials ZIF-8@PVPA (85:15) (1) and ZIF-8@PVPA (75:25) (2). The mechanism for the formation of the hollow nanostructures, which may be similar to the Kirkendall effect, was also briefly investigated. The obtained hollow nanostructures exhibit remarkably high proton conductivities under high-temperature, anhydrous conditions.

2. EXPERIMENTAL SECTION

Materials. 2-Methylimidazole (Hmim with 97% purity) and zinc nitrate hexahydrate ($Zn(NO_3)_2{\cdot}6H_2O$, 99% purity—metal based) were purchased from Alfa Aesar. Poly(vinylphosponic acid) (PVPA, 30% solution) was obtained from Polysciences, Inc. Methanol with 99.9% purity was purchased from Merck.

Synthesis of ZIF-8 Nanoparticles. In the synthesis of the ZIF-8 nanoparticles, a reported procedure was followed.[39] A solution of 4.2 g (14.12 mmol) $Zn(NO_3)_2{\cdot}6H_2O$ in 200 mL of methanol was poured into a solution of 9.36 g (113.2 mmol) Hmim in 200 mL of methanol. Then, the resulting solution was vigorously stirred at room temperature for 1 h. At the end of the stirring process, the milky solution was centrifuged at 7500 rpm, 15 min, two times, to obtain the desired nanoparticles, which were washed by methanol. Finally, some part was heated in a vacuum oven at 80 °C for 24 h for further characterization, and the rest of the nanoparticles were suspended in methanol for the next steps. The yield of ZIF-8 synthesis was ∼30% based on Zn.

Synthesis of ZIF-8@PVPA Hollow Hybrid Nanostructures. Hollow hybrid nanostructures were fabricated by physical blending methods at room temperature under ambient conditions. Typically, 0.5 g PVPA (30 wt % aqueous solution) was diluted to 1 wt % with the addition of deionized water and heated to 80 °C. Solution was stirred for 1 h until homogeneity was obtained. Afterward, a certain amount of PVPA solution was added to ZIF-8 nanoparticles suspended in methanol by a buret slowly. And then, final solution was mechanically stirred for 1 h at room temperature. Afterwards, the mother solution was removed by centrifuging at 7500 rpm, 20 min. The ZIF-8@PVPA hollow nanostructures were collected, washed with methanol three times, and centrifuged to separate liquid from the solid each time. The product was dried in a vacuum oven at 80 °C for 24 h.

Characterization. Scanning electron microscopy (SEM) images were acquired on a Hitachi SU8030 SEM. Thermogravimetric analysis (TGA) were performed on a TGA/DSC system (Mettler-Toledo AG, Schwerzenbach, Switzerland), which runs on a PC with STAR e software. Samples were heated from 25 to 900 °C at 10 °C/min rate under N_2 flow. Powder X-ray diffraction (PXRD) patterns were recorded on a Rigaku ATXG diffractometer equipped with an 18 kW Cu rotating anode, MLO monochromator, and a high-count-rate scintillation detector (measurements made over a range of $1.5° < 2\theta < 40°$ in 0.05° step width with a 2°/min scanning speed). The solid was dried in a vacuum oven at 80 °C for 2 h and activated at 100 °C for 12 h on a SmartVacPrep instrument (Micromeritics Instrument Corporation, Norcross, GA, USA). All N_2 isotherms were measured on a Micromeritics Tristar II (Micromeritics, Norcross, GA, USA). Measurements were performed at 77 K, with the temperature held constant using a liquid N_2 bath. Consistency criteria were adapted to choose the pressure range selection for BET calculation. Conductivities were measured by the AC impedance method using an electrochemical instrument (Gamry Interface 1000) in the frequency range of 1 MHz to 1 Hz at AC amplitude of 100 mV. For the powder conductivity measurements, 80−100 mg of powder was gently ground using a pestle and mortar, and then was pressed into a pellet. The conductivity measurements were performed for sandwiched pellets by Pt electrodes. Transmission electron microscope (TEM) images were taken by a JEOL JEM 2010F at an accelerating voltage of 200 kV. The JEOL JEM 2010F is also equipped with an energy dispersive X-ray spectrometer (EDX) system and facilitates the elemental analysis of samples. Attenuated total reflectance Fourier transform spectroscopy (ATR-FTIR) spectra were recorded on a Nicolet 7600. The obtained spectrum with 4 cm^{-1} resolution is between 400 and 4000 cm^{-1}.

DOI: 10.1021/acsami.6b05901
ACS Appl. Mater. Interfaces 2016, 8, 23015−23021

3. RESULTS AND DISCUSSION

Characterization of Hybrids. Powder X-ray (PXRD) measurements were carried out for ZIF-8 nanoparticles and ZIF-8@PVPA hybrid materials with different ZIF-8 loadings (Figure 1). The diffraction peaks of the ZIF-8 nanoparticles

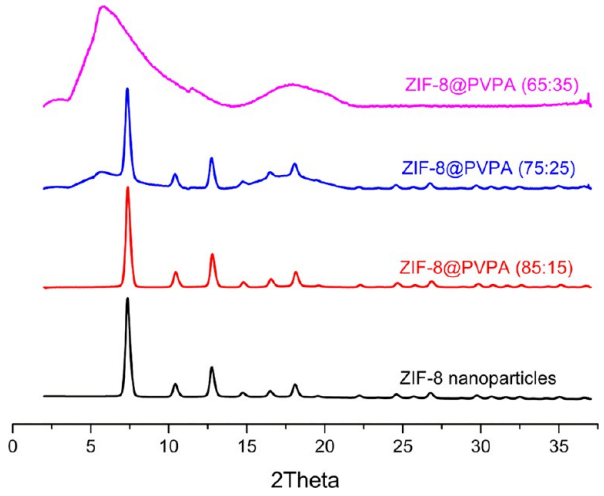

Figure 1. Normalized PXRD patterns of ZIF-8 NPs and ZIF-8@PVPA hollow nanostructures.

(NPs) were well matched with the known XRD pattern for bulk ZIF-8.[32] The XRD patterns of ZIF-8@PVPA (85:15) and ZIF-8@PVPA (75:25) are also a characteristic feature of diffraction peaks matching those of bulk ZIF-8, indicating that both hybrid materials contain crystalline MOF material. It should be noted, however, that increasing the PVPA content in the hybrid nanostructures diminishes and weakens peaks corresponding to ZIF-8. Based on these results, we conclude that some of ZIF-8 NPs likely disintegrate, a point that is discussed further below. The XRD pattern of ZIF-8@PVPA (65:35) shows a divergence from crystallinity, suggesting that the majority of the initially present ZIF-8 NPs had decomposed in the inherently acidic medium used. SEM and TEM images of ZIF-8@PVPA (65:35) (Figure S1) reveal that the majority of ZIF-8@PVPA (65:35) is composed of ill-defined particles and aggregates. Given these results, only findings for ZIF-8@PVPA (85:15) and ZIF-8@PVPA (75:25) are included in the following discussions.

ATR/FT-IR was used to better understand the bonding interactions between ZIF-8 and PVPA in **1** and **2** (Figure S2). In the spectrum of ZIF-8@PVPA, the peaks at 1052, 992, and 901 cm^{-1} were assigned to (P═O) stretching and asymmetric and symmetric vibrations of (P−O), respectively, in the PVPA.[37] As expected, the intensities of these peaks increased with increasing amounts of PVPA. The peaks at 2974 and 1586 cm^{-1} are assigned to (C−H) and (C═N) stretches in ZIF-8, while peaks at 747 and 667 cm^{-1} are attributed to (Zn−O) and (Zn−N) stretches, respectively,[32,34] Together these data indicate that ZIF-8 is present in both composites.

The porosity of ZIF-8 NPs compared to the ZIF-8@PVPA hybrid hollow nanostructures was determined via N_2 isotherm measurements at 77 K (Figure 2). The specific surface areas (BET areas) for ZIF-8 NPs, **1**, and **2** were found to be 1770, 145, and 50 $m^2\ g^{-1}$, respectively. This dramatic decrease in accessible surface area implies that the pores in the MOF are

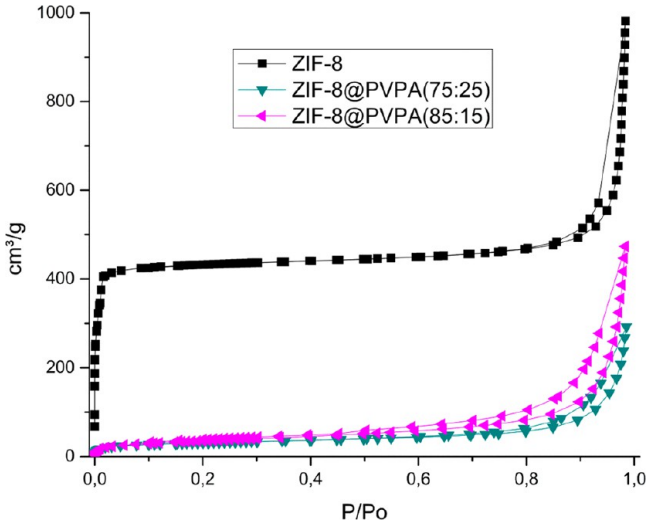

Figure 2. Nitrogen physisorption isotherms of pure ZIF-8 NPs and ZIF-8@PVPA hollow nanostructures measured at 77 K.

blocked by the nonporous polymer, PVPA, in the newly formed structures.

Scanning electron microscopy (SEM) and transmission electron microscopy (TEM) were used to follow the formation of the MOF/polymer hybrid and, specifically, the formation of hollow nanostructures. As shown in Figure 3a and d, before mixing, the pristine ZIF-8 NPs are monodisperse well-defined rhombic-dodecahedral-shaped nanocrystals with an average diameter of 60 nm.[39] Addition of PVPA to ZIF-8 in MeOH, with stirring, was followed within 2 min by PVPA encapsulation of the NPs (Figure 3b and e). Micrographs recorded after 1 h of mechanical mixing revealed that the composite had evolved from a conventional core(MOF)/shell(polymer) structure to one characterized by a hollow core and an apparently single-phase and morphologically uniform shell that retains the shape of the MOF nanoparticles (Figure 3c and f). Elemental mapping via energy dispersive X-ray spectroscopy (EDS) confirmed the presence of phosphorus and zinc. EDS also established that the two elements are found (and uniformly distributed) in the shells and essentially absent from the apparent voids, consistent with a description of the hybrid as a collection of hollow nanoparticles; see Figure S4. TEM images of ZIF-8 NPs, ZIF-8@PVPA (85:15), and ZIF-8@PVPA (75:25) obtained at various magnifications are shown in Figure 4. The hollow morphology could be observed in both ZIF-8@PVPA (85:15) and ZIF-8@PVPA (75:25), and the thickness of the shell increased with increasing PVPA content in the structure (Figure 4).

Formation of Hybrid Hollow Nanostructures. The unexpected formation of hollow nanostructures is reminiscent of the well-known Kirkendall effect.[40−43] The effect is typically observed with metals that are initially arranged with one metal constituting a core and a second constituting a shell. If the atomic diffusity of the core element (A) greatly exceeds that of the element (B) constituting the coating, an AB compound begins to form at the boundary between core and coating. The difference in diffusivities ensures that the AB compound grows on the B side of the boundary. Provided that sufficient numbers of B atoms are available to sustain AB formation, the vacancies formed on the A side will eventually define a hollow interior that is bounded by an AB shell and that matches the shape and size of the original A core.[40,41]

DOI: 10.1021/acsami.6b05901
ACS Appl. Mater. Interfaces 2016, 8, 23015−23021

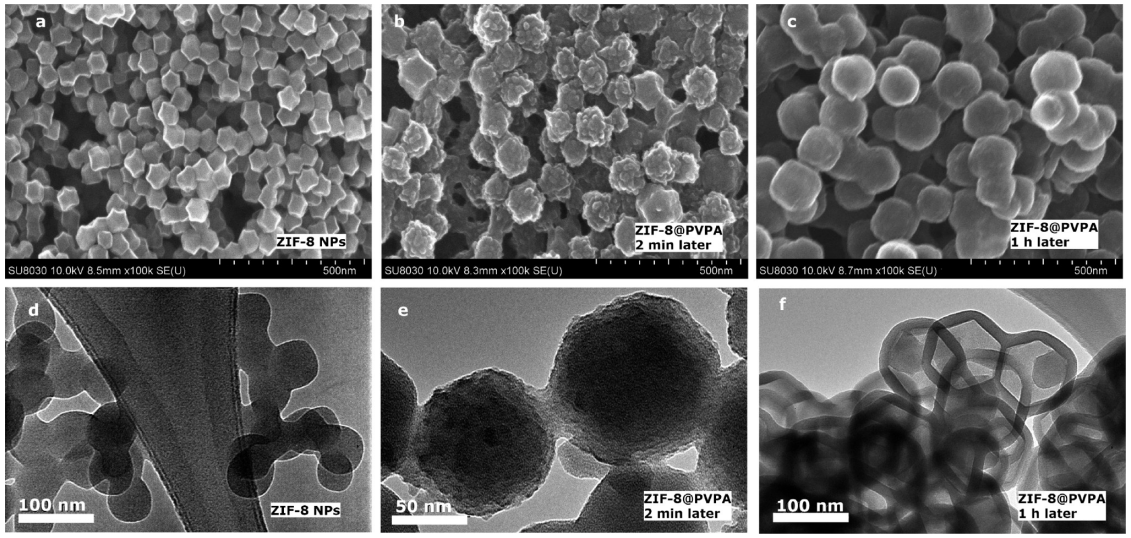

Figure 3. SEM (a,b,c) and TEM (d,e,f) images of ZIF@PVPA hollow nanostructures for the formation. Images were taken from (a,d) ZIF-8 NPs and samples collected after mechanically stirring the mixed solution of ZIF-8 NPs and PVPA for (b,e) 2 and (c,f) 60 min.

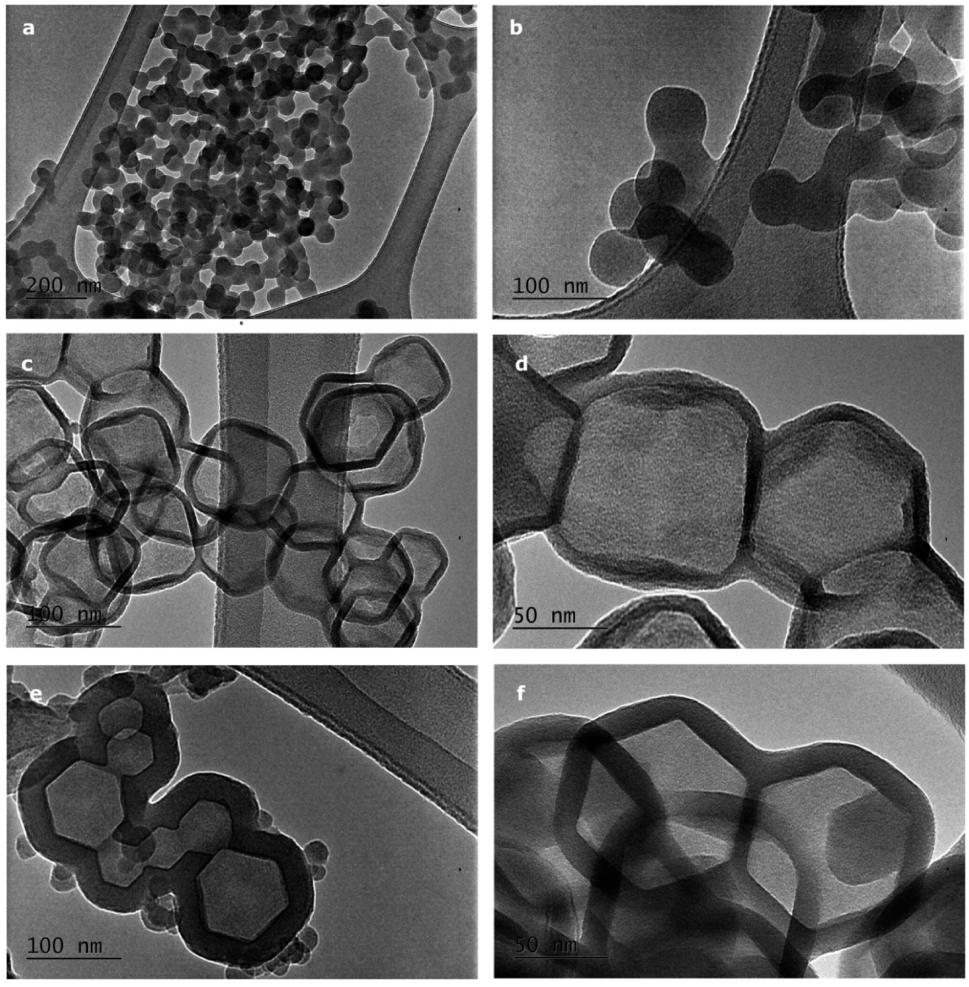

Figure 4. TEM images of ZIF-8 NPs and ZIF-8@PVPA hollow nanostructures. (a,b) ZIF-8 NPs, (c,d) ZIF-8@PVPA (85:15), and (e,f) ZIF-8@PVPA (75:25).

We propose that a qualitatively similar process occurs after PVPA enshrouds nanoparticles of ZIF-8. Figure 5 presents a simplified illustration. As for the details, it is worth noting that the apertures of ZIF-8 are too small to directly accommodate PVPA. Thus, a mechanism for composite shell formation based on simple permeation of the MOF can be ruled out. It is also worth noting that phosphonates bind to Zn(II) much more strongly than do azolates. Indeed, phosphonates can display

DOI: 10.1021/acsami.6b05901
ACS Appl. Mater. Interfaces 2016, 8, 23015−23021

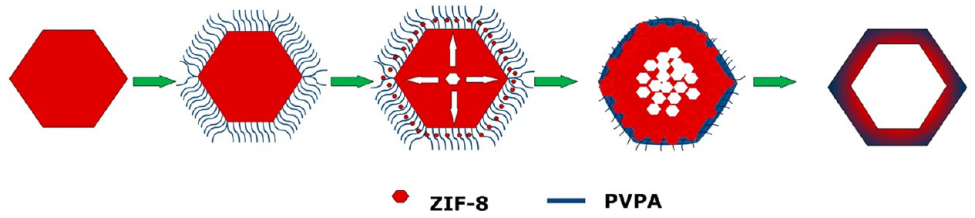

Figure 5. Proposed scheme (simplified) for the formation of ZIF-8@PVPA hollow nanostructures.

imidazolates from the coordination sphere of Zn(II). To the extent that displacement (ligand substitution) occurs here, the ZIF-8 nanocrystals will be fragmented and pulled into regions defining shells. The absence of easily observable granularity in the shells (see Figure 4c–f) implies that fragmentation is extensive and that fragments have dimensions of several nanometers or less.

Returning to the molecular-scale coordination chemistry, replacement of 2-methyl-imidazolate ligands (mim^{-1}) by phosphonate groups is anticipated to yield free or partially free methyl-imidazole (Hmim) and/or free methyl-imidazolium ($HmimH^+$). At the same time, tying up a phosphonate group with Zn(II) precludes that group from later condensing with a neighboring phosphonic acid and forming an anhydride.

Finally, TGA and DTG measurements showed that ZIF-8 NPs are thermally stable up to 550 °C under nitrogen[32,39] (Figure S3). In contrast, the first weight loss in unblended PVPA begins at about 130 °C and has been shown to be due to the condensation of phosphonic acid moieties.[4,37] (As noted above, condensation (i.e., formation of anhydrides) greatly diminishes the proton conductivity of PVPA.) Blending and composite formation results in remarkable increases in decomposition temperature −250 °C for ZIF-8@PVPA (75:25), for example, and thus a remarkable suppression of functional-group condensation. The suppression may be a consequence of strong hydrogen-bonding between phosphonic acid groups and components of ZIF-8, isolation of otherwise proximal phosphonic acid groups by composite formation, conversion of phosphonic acid groups to noncondensable zinc-coordinated phosphonates, or all three. Regardless, the absence of condensation at temperatures below ∼250 °C suggested to us that the composites, in contrast to pure PVPA, might well display high proton conductivity under anhydrous conditions and at temperatures well above 100 °C. We will explore this idea in the next section.

Proton Conductivity. Anhydrous proton conductivity measurements were performed on the hybrids between 50 and 140 °C. As can be seen in Figure 6, conductivities increase with temperature and with PVPA content; the temperature dependences fit Arrhenius behavior. The highest value obtained for the proton conductivity of **2**, $\sigma = 3.2\ (\pm 0.12) \times 10^{-3}$ S cm^{-1} at T = 140 °C under anhydrous conditions, is slightly higher than that reported for a neat PVPA membrane, $\sigma = 10^{-3}$ S cm^{-1} at T = 150 °C[5,37] and considerably higher than that of pure ZIF-8, $\sigma = 4.6 \times 10^{-4}$ S cm^{-1} at T = 94 °C and RH = 98%.[44] However, the proton conductivity for **1**, $\sigma = 1\ (\pm 0.12) \times 10^{-4}$ S cm^{-1} at T = 140 °C under anhydrous conditions, consistent with lower PVPA content.

The observation of conductivity values for **2** that exceed those for pure PVPA suggests a role for conductivity-enhancing protogenic groups. The ideal protogenic group should have both proton donor and acceptor facilities; it should be sufficiently amphoteric in a Brønsted sense to achieve

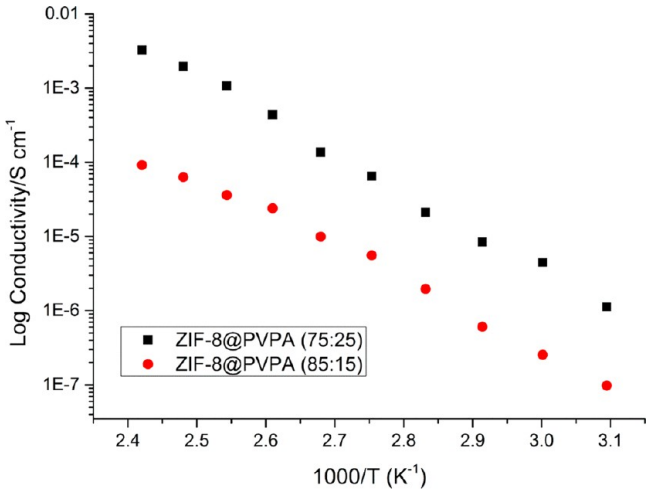

Figure 6. Arrhenius plots of proton conductivities of ZIF-8@PVPA hollow nanostructures.

significant self-dissociation.[5,35,45] Phosphonic acid groups ($-PO_3H_2$) can act as both proton donors (via P−O−H) and proton acceptors (via (P═O)).[5,36,37] Linker termination of the ZIF-8 NPs yields exposed Hmim units which can similarly act as proton donors (sharing protons on N−H) and proton acceptors (through noncoordinated N atoms).[32] (Also likely present are free Hmim and/or $HmimH^+$ species, i.e., byproducts of phosphonate substitution at zinc centers.) The amphotericity of the constituents in the hybrid hollow structures should permit them to form a strong hydrogen-bonding network.

A proposed (simplified) pathway for proton transfer mechanism for ZIF-8@PVPA hollow nanostructures is shown in Figure 7b. Two modes of proton transfer are envisaged: Either PVPA acts as the proton donor and ZIF-8 acts as a proton acceptor, or ZIF-8 acts as a proton donor that assists proton transport between neighboring phosphonic acid groups. In this way, protons donated by PVPA (or ZIF-8) can be transferred via the formation and breaking of hydrogen bonds over a pathway which is distributed throughout the ZIF-8–PVPA shell. From the conductivity data in Figure S6, the activation energies for proton transport through **1** and **2**, respectively, are 37 and 46 kJ mol^{-1} (0.39 and 0.47 eV); see SI. These values are consistent with those from published studies of PVPA blends at high temperatures and under low-humidity conditions.[4,5,32,37] In those studies, the dominant proton transfer mechanism is the Grotthuss (or hopping) mechanism.

4. CONCLUSIONS

The formation of proton-conducting ZIF-8@PVPA hybrid hollow nanostructures can be initiated by simple physical blending of ZIF-8 nanoparticles and PVPA in methanol; formation is complete within an hour. The mechanism by

DOI: 10.1021/acsami.6b05901
ACS Appl. Mater. Interfaces 2016, 8, 23015−23021

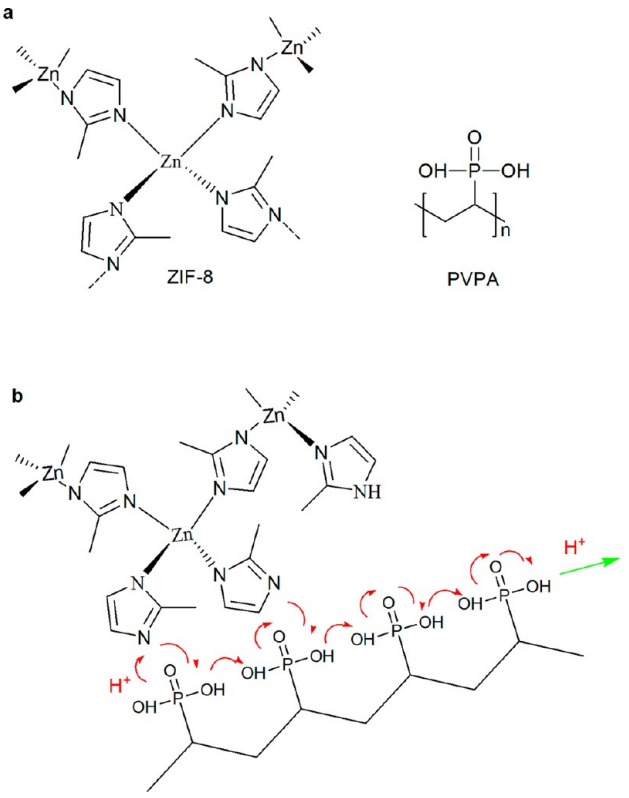

Figure 7. (a) Chemical structures of ZIF-8 and PVPA. (b) Potential mechanism for proton transfer in ZIF-8@PVPA hollow nanostructures. For simplicity, free Hmim, free $HmimH^+$, and zinc-coordinated phosphonates are omitted from the scheme.

which the hollow nanostructures form can be explained by invoking the Kirkendall effect, with ZIF-8 constituting the diffusively mobile component. The effect, as manifested here, entails fragmentation of initially encapsulated MOF nanoparticles and diffusive transport of fragments into shells comprising immobile PVPA. The nanoparticle fragmentation is likely driven by strong hydrogen bonding between phosphonic acid groups and crystallite-terminating imidazoles or imidazolates, as well as by coordinative displacement of imidazolate linkers by polymer-pendant phosphonate groups at some of the Zn(II) nodes in ZIF-8. That not all zinc ions react is evidenced by the retention of ZIF-8 peaks in the XRD spectra of the hybrid compounds.

The hybrids display good proton conductivity—values as high as $\sigma = 3.2 \times 10^{-3}$ S cm^{-1}, which exceed those of either pure ZIF-8 or pure PVPA. Measurements of apparent activation energies yield values that are typical of Grotthus-type transport. The conductivity enhancement for the hybrid is attributed to the availability of amphoteric moieties (phosphonic acid, free methyl-imidazole, and partially zinc-ligated methyl-imidazole) from both components of the reactive blend. In contrast to the behavior of PVPA itself, the high conductivity of the hybrid persists even at high temperature under anhydrous conditions—a finding that holds promise for the potential application of the hybrids in PEM fuel cells. The basis for persistence of conductivity is the inhibition of formation of nonconductive phosphoanhydride species. Strong hydrogen bonding between PVPA and the exterior surfaces ZIF-8 fragments, together with zinc(II)-coordination of a fraction of the available phosphonate (phosphonic acid) units, likely accounts for the remarkable resistance of the hybrids to self-condensation (anhydride formation).

Going forward, it will be interesting to evaluate the performance of membranes based on the hybrid compounds. Also of interest may be hybrids based on PVPA and other ZIF compounds, especially those assembled from functionalized imidazoles (imidazolates) characterized by pK_a's, pK_b's, and hydrogen-bonding propensities that differ from those 2-methylimidazole, as these modulate conductivity.

■ ASSOCIATED CONTENT

Supporting Information

The Supporting Information is available free of charge on the ACS Publications website at DOI: 10.1021/acsami.6b05901.

Characterization for hollow hybrid nanostructures; calculation of activation energy (PDF)

■ AUTHOR INFORMATION

Corresponding Authors

*E-mail: unal.sen@agu.edu.tr.
*E-mail: j-hupp@northwestern.edu.
*E-mail: o-farha@northwestern.edu.

Notes

The authors declare no competing financial interest.

■ ACKNOWLEDGMENTS

The work performed at Abdullah Gul University was funded by The Scientific and Technological Research Council of Turkey TUBITAK under the contract No. 214M397. For work done in Evanston, we gratefully acknowledge support from the U.S. Dept. of Energy, Office of Science, Office of Basic Energy Sciences (grant no. DE-FG02-87ER13808) and Northwestern University.

■ REFERENCES

(1) Jimenez-Garcia, L.; Kaltbeitzel, A.; Pisula, W.; Gutmann, J. S.; Klapper, M.; Mullen, K. Phosphonated Hexaphenylbenzene: A Crystalline Proton Conductor. *Angew. Chem., Int. Ed.* **2009**, *48*, 9951−9953.

(2) Wehmeyer, C.; Schrader, M.; Andrienko, D.; Sebastiani, D. Water-Free Proton Conduction in Hexakis(P-Phosphonatophenyl)-Benzene Nanochannels. *J. Phys. Chem. C* **2013**, *117*, 12366−12372.

(3) Chandan, A.; Hattenberger, M.; El-Kharouf, A.; Du, S. F.; Dhir, A.; Self, V.; Pollet, B. G.; Ingram, A.; Bujalski, W. High Temperature (Ht) Polymer Electrolyte Membrane Fuel Cells (Pemfc) - A Review. *J. Power Sources* **2013**, *231*, 264−278.

(4) Wang, C.; Paddison, S. J. Proton Transfer in Functionalized Phosphonic Acid Molecules. *Phys. Chem. Chem. Phys.* **2010**, *12*, 970−981.

(5) Steininger, H.; Schuster, M.; Kreuer, K. D.; Kaltbeitzel, A.; Bingol, B.; Meyer, W. H.; Schauff, S.; Brunklaus, G.; Maier, J.; Spiess, H. W. Intermediate Temperature Proton Conductors for Pem Fuel Cells Based on Phosphonic Acid as Protogenic Group: A Progress Report. *Phys. Chem. Chem. Phys.* **2007**, *9*, 1764−1773.

(6) Li, S. W.; Zhou, Z.; Zhang, Y. L.; Liu, M. L.; Li, W. 1h-1,2,4-Triazole: An Effective Solvent for Proton-Conducting Electrolytes. *Chem. Mater.* **2005**, *17*, 5884−5886.

(7) Sen, U.; Unugurcelik, S.; Ata, A.; Bozkurt, A. Anhydrous Proton Conducting Membranes for Pem Fuel Cells Based on Nafion/Azole Composites. *Int. J. Hydrogen Energy* **2008**, *33*, 2808−2815.

(8) Kim, J. D.; Oba, Y.; Ohnuma, M.; Jun, M. S.; Tanaka, Y.; Mori, T.; Choi, Y. W.; Yoon, Y. G. Physico-Chemical Properties of Highly Flexible Temperature Tolerant Anhydrous Nafion-1,2,3-Triazole Blend Membranes. *J. Electrochem. Soc.* **2010**, *157*, B1872−B1877.

DOI: 10.1021/acsami.6b05901
ACS Appl. Mater. Interfaces 2016, 8, 23015−23021

(9) Sen, U.; Bozkurt, A.; Ata, A. Nafion/Poly(1-Vinyl-1,2,4-Triazole) Blends as Proton Conducting Membranes for Polymer Electrolyte Membrane Fuel Cells. *J. Power Sources* **2010**, *195*, 7720−7726.
(10) Bennett, T. D.; Cheetham, A. K. Amorphous Metal-Organic Frameworks. *Acc. Chem. Res.* **2014**, *47*, 1555−1562.
(11) Furukawa, H.; Cordova, K. E.; O'Keeffe, M.; Yaghi, O. M. The Chemistry and Applications of Metal-Organic Frameworks. *Science* **2013**, *341*, 974.
(12) Farha, O. K.; Hupp, J. T. Rational Design, Synthesis, Purification, and Activation of Metal-Organic Framework Materials. *Acc. Chem. Res.* **2010**, *43*, 1166−1175.
(13) Horike, S.; Shimomura, S.; Kitagawa, S. Soft Porous Crystals. *Nat. Chem.* **2009**, *1*, 695−704.
(14) Ferey, G. Hybrid Porous Solids: Past, Present, Future. *Chem. Soc. Rev.* **2008**, *37*, 191−214.
(15) Farha, O. K.; Yazaydin, A. O.; Eryazici, I.; Malliakas, C. D.; Hauser, B. G.; Kanatzidis, M. G.; Nguyen, S. T.; Snurr, R. Q.; Hupp, J. T. De Novo Synthesis of a Metal-Organic Framework Material Featuring Ultrahigh Surface Area and Gas Storage Capacities. *Nat. Chem.* **2010**, *2*, 944−948.
(16) Furukawa, H.; Ko, N.; Go, Y. B.; Aratani, N.; Choi, S. B.; Choi, E.; Yazaydin, A. O.; Snurr, R. Q.; O'Keeffe, M.; Kim, J.; Yaghi, O. M. Ultrahigh Porosity in Metal-Organic Frameworks. *Science* **2010**, *329*, 424−428.
(17) Alezi, D.; Belmabkhout, Y.; Suyetin, M.; Bhatt, P. M.; Weselinski, L. J.; Solovyeva, V.; Adil, K.; Spanopoulos, I.; Trikalitis, P. N.; Emwas, A. H.; Eddaoudi, M. Mof Crystal Chemistry Paving the Way to Gas Storage Needs: Aluminum-Based Soc-Mof for Ch4, O-2, and CO2 Storage. *J. Am. Chem. Soc.* **2015**, *137*, 13308−13318.
(18) Peng, Y.; Krungleviciute, V.; Eryazici, I.; Hupp, J. T.; Farha, O. K.; Yildirim, T. Methane Storage in Metal-Organic Frameworks: Current Records, Surprise Findings, and Challenges. *J. Am. Chem. Soc.* **2013**, *135*, 11887−11894.
(19) Lee, J.; Farha, O. K.; Roberts, J.; Scheidt, K. A.; Nguyen, S. T.; Hupp, J. T. Metal-Organic Framework Materials as Catalysts. *Chem. Soc. Rev.* **2009**, *38*, 1450−1459.
(20) Gascon, J.; Corma, A.; Kapteijn, F.; Llabres i Xamena, F. X. Metal Organic Framework Catalysis: Quo Vadis? *ACS Catal.* **2014**, *4*, 361−378.
(21) Farrusseng, D.; Aguado, S.; Pinel, C. Metal-Organic Frameworks: Opportunities for Catalysis. *Angew. Chem., Int. Ed.* **2009**, *48*, 7502−7513.
(22) Ramaswamy, P.; Wong, N. E.; Shimizu, G. K. H. Mofs as Proton Conductors - Challenges and Opportunities. *Chem. Soc. Rev.* **2014**, *43*, 5913−5932.
(23) Tominaka, S.; Cheetham, A. K. Intrinsic and Extrinsic Proton Conductivity in Metal-Organic Frameworks. *RSC Adv.* **2014**, *4*, 54382−54387.
(24) Taylor, J. M.; Dawson, K. W.; Shimizu, G. K. H. A Water-Stable Metal-Organic Framework with Highly Acidic Pores for Proton-Conducting Applications. *J. Am. Chem. Soc.* **2013**, *135*, 1193−1196.
(25) Taylor, J. M.; Dekura, S.; Ikeda, R.; Kitagawa, H. Defect Control to Enhance Proton Conductivity in a Metal−Organic Framework. *Chem. Mater.* **2015**, *27*, 2286−2289.
(26) Sadakiyo, M.; Yamada, T.; Kitagawa, H. Proton Conductivity Control by Ion Substitution in a Highly Proton-Conductive Metal - Organic Framework. *J. Am. Chem. Soc.* **2014**, *136*, 13166−13169.
(27) Bureekaew, S.; Horike, S.; Higuchi, M.; Mizuno, M.; Kawamura, T.; Tanaka, D.; Yanai, N.; Kitagawa, S. One-Dimensional Imidazole Aggregate in Aluminium Porous Coordination Polymers with High Proton Conductivity. *Nat. Mater.* **2009**, *8*, 831−836.
(28) Hurd, J. A.; Vaidhyanathan, R.; Thangadurai, V.; Ratcliffe, C. I.; Moudrakovski, I. L.; Shimizu, G. K. H. Anhydrous Proton Conduction at 150 Degrees C in a Crystalline Metal-Organic Framework. *Nat. Chem.* **2009**, *1*, 705−710.
(29) Horike, S.; Umeyama, D.; Kitagawa, S. Ion Conductivity and Transport by Porous Coordination Polymers and Metal-Organic Frameworks. *Acc. Chem. Res.* **2013**, *46*, 2376−2384.
(30) Liu, S. C.; Yue, Z. F.; Liu, Y. Incorporation of Imidazole within the Metal-Organic Framework Uio-67 for Enhanced Anhydrous Proton Conductivity. *Dalton T* **2015**, *44*, 12976−12980.
(31) Yamada, T.; Otsubo, K.; Makiura, R.; Kitagawa, H. Designer Coordination Polymers: Dimensional Crossover Architectures and Proton Conduction. *Chem. Soc. Rev.* **2013**, *42*, 6655−6669.
(32) Erkartal, M.; Usta, H.; Citir, M.; Sen, U. Proton Conducting Poly(Vinyl Alcohol) (Pva)/Poly (2-Acrylamido-2-Methylpropane Sulfonic Acid) (Pamps)/Zeolitic Imidazolate Framework (Zif) Ternary Composite Membrane. *J. Membr. Sci.* **2016**, *499*, 156−163.
(33) Liang, X. Q.; Zhang, F.; Feng, W.; Zou, X. Q.; Zhao, C. J.; Na, H.; Liu, C.; Sun, F. X.; Zhu, G. S. From Metal-Organic Framework (Mof) to Mof-Polymer Composite Membrane: Enhancement of Low-Humidity Proton Conductivity. *Chem. Sci.* **2013**, *4*, 983−992.
(34) Wu, B.; Pan, J. F.; Ge, L.; Wu, L.; Wang, H. T.; Xu, T. W. Oriented Mof-Polymer Composite Nanofiber Membranes for High Proton Conductivity at High Temperature and Anhydrous Condition. *Sci. Rep.* **2014**, *4*, 4334 DOI: 10.1038/srep04334.
(35) Kreuer, K. D.; Paddison, S. J.; Spohr, E.; Schuster, M. Transport in Proton Conductors for Fuel-Cell Applications: Simulations, Elementary Reactions, and Phenomenology. *Chem. Rev.* **2004**, *104*, 4637−4678.
(36) Schuster, M.; Rager, T.; Noda, A.; Kreuer, K. D.; Maier, J. About the Choice of the Protogenic Group in Pem Separator Materials for Intermediate Temperature, Low Humidity Operation: A Critical Comparison of Sulfonic Acid, Phosphonic Acid and Imidazole Functionalized Model Compounds. *Fuel Cells* **2005**, *5*, 355−365.
(37) Sen, U.; Acar, O.; Celik, S. U.; Bozkurt, A.; Ata, A.; Tokumasu, T.; Miyamoto, A., Proton-Conducting Blend Membranes of Nafion/Poly(Vinylphosphonic Acid) for Proton Exchange Membrane Fuel Cells. *J. Polym. Res.* **2013**, *20*; 10.1007/s10965-013-0217-2
(38) Huo, J.; Marcello, M.; Garai, A.; Bradshaw, D. Mof-Polymer Composite Microcapsules Derived from Pickering Emulsions. *Adv. Mater.* **2013**, *25*, 2717−2722.
(39) Cravillon, J.; Munzer, S.; Lohmeier, S. J.; Feldhoff, A.; Huber, K.; Wiebcke, M. Rapid Room-Temperature Synthesis and Characterization of Nanocrystals of a Prototypical Zeolitic Imidazolate Framework. *Chem. Mater.* **2009**, *21*, 1410−1412.
(40) Wang, W. S.; Dahl, M.; Yin, Y. D. Hollow Nanocrystals through the Nanoscale Kirkendall Effect. *Chem. Mater.* **2013**, *25*, 1179−1189.
(41) Yin, Y. D.; Rioux, R. M.; Erdonmez, C. K.; Hughes, S.; Somorjai, G. A.; Alivisatos, A. P. Formation of Hollow Nanocrystals through the Nanoscale Kirkendall Effect. *Science* **2004**, *304*, 711−714.
(42) Gao, R.; Chen, M.; Li, W.; Zhou, S. X.; Wu, L. M. Facile Fabrication and Some Specific Properties of Polymeric/Inorganic Bilayer Hybrid Hollow Spheres. *J. Mater. Chem. A* **2013**, *1*, 2183−2191.
(43) Jin Fan, H.; Knez, M.; Scholz, R.; Nielsch, K.; Pippel, E.; Hesse, D.; Zacharias, M.; Gosele, U. Monocrystalline Spinel Nanotube Fabrication Based on the Kirkendall Effect. *Nat. Mater.* **2006**, *5*, 627−631.
(44) Barbosa, P.; Rosero-Navarro, N. C.; Shi, F. N.; Figueiredo, F. M. L. Protonic Conductivity of Nanocrystalline Zeolitic Imidazolate Framework 8. *Electrochim. Acta* **2015**, *153*, 19−27.
(45) Graf, R. New Proton Conducting Materials for Technical Applications: What Can We Learn from Solid State Nmr Studies? *Solid State Nucl. Magn. Reson.* **2011**, *40*, 127−133.

DOI: 10.1021/acsami.6b05901
ACS Appl. Mater. Interfaces 2016, 8, 23015−23021